COMPARING THE VARIATIONAL APPROXIMATION AND EXACT SOLUTIONS OF THE STRAIGHT UNSTAGGERED AND TWISTED STAGGERED DISCRETE SOLITONS

by

DANIEL E. MARULANDA
B.S. Stetson University, 2013

A thesis submitted in partial fulfilment of the requirements
for the degree of Master of Science
in the Department of Mathematics
in the College of Sciences
at the University of Central Florida
Orlando, Florida

Summer Term
2016

Major Professor: D.J. Kaup

ABSTRACT

Discrete nonlinear Schrödinger equations (DNSL) have been used to provide models of a variety of physical settings. An application of DNSL equations is provided by Bose-Einstein condensates which are trapped in deep optical-lattice potentials. These potentials effectively splits the condensate into a set of droplets held in local potential wells, which are linearly coupled across the potential barriers between them [3]. In previous works, DNLS systems have also been used for symmetric on-site-centered solitons [11]. A few works have constructed different discrete solitons via the *variational approximation* (VA) and have explored their regions for their solutions [11, 12]. Exact solutions for *straight unstaggered-twisted staggered* (SUTS) discrete solitons have been found using the shooting method [12].

In this work, we will use Newton's method, which converges to the exact solutions of SUTS discrete solitons. The VA has been used to create starting points. There are two distinct types of solutions for the soliton's waveform: SUTS discrete solitons and straight unstaggered discrete solitons, where the twisted component is zero in the latter soliton. We determine the range of parameters for which each type of solution exists. We also compare the regions for the VA solutions and the exact solutions in certain selected cases. Then, we graphically and numerically compare examples of the VA solutions with their corresponding exact solutions. We also find that the VA provides reasonable approximations to the exact solutions.

For my family and the people that have guided me along the way.

TABLE OF CONTENTS

LIST OF FIGURES

CHAPTER 1: INTRODUCTION

The discrete nonlinear Schrödinger equations (DNLS) have been prominent in the description of numerous experiments in applied nonlinear sciences. The DNLS equations have also been implements for other physical settings in efforts to make accurate predictions [9] . An example of this is provided by Bose-Einstein condensates which are trapped in deep optical-lattice potentials. These potentials effectively split the condensate into a set of droplets held in local potential wells, which are linearly coupled across the potential barriers between them [3, 4]. Ref. [7] demonstrates how the DNLS equations can be used for many other models and applications.

The DNLS equations that we study have self-attractive and self-repulsive on-site nonlinearities where one mode is unstaggered and the other is staggered. Unstaggered solitons do not have the sign alteration at adjacent sites of the lattice field whereas staggered solitons do have sign alterations, as shown in Figure 1.1. In the continuum limit, the unstaggered solitons correspond to regular solitons, while the staggered solitons may be considered as counterparts of gap solitons [8].

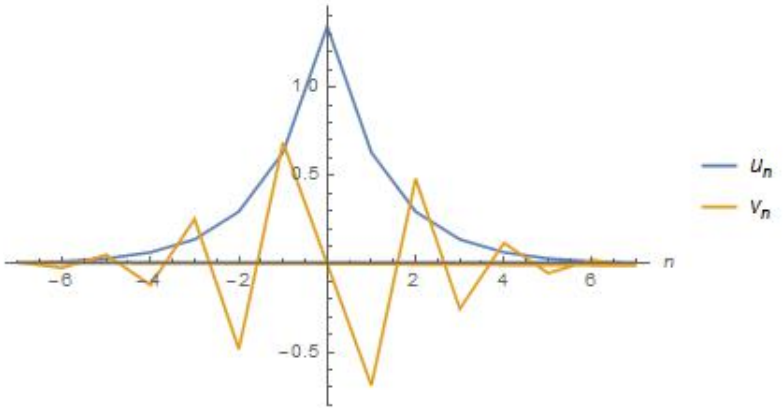

Figure 1.1: u_n components are unstaggered and have $u_{-n} = u_n$. Whereas v_n components are staggered and have opposite signs of the lattice field at adjacent sites.

Ref. [11], studied the solutions of the DNLS for symmetric on-site centered solitons with mixed staggered and unstaggered components. An example of this, is the discrete solutions of the mixed type, constructed with unstaggered and staggered components. Once unstaggered-staggered discrete solitons are understood using a two component DNLS system, the next level gives rise to the possibility of working with antisymmetric twisted solitons. In this thesis, we want to study the *straight unstaggered-twisted staggered* (SUTS) discrete solitons for the DNLS. The form of the SUTS discrete solitions are shown in Figure 1.2. To study this case, we first start with the Variational Approximation (VA) as starting points and then apply the Newton method to obtain exact solutions for each value of u_n and v_n components. We define exact solutions of u_n and v_n to be the values of u_n and v_n for which the stationary equations, Eq. (2.6) and Eq. (2.7), are less than 10^{-7}.

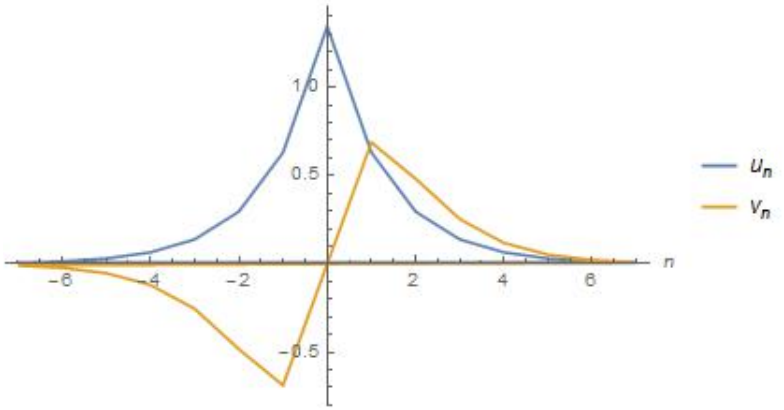

Figure 1.2: Straight Unstaggered components do not have the sign alternation at adjacent sites of the lattice fields. The twisted component is negative for negative values of n, positive for positive values of n and zero for $n = 0$.

The VA can be used for any set of discrete functions. In [12] it has been used to approximate the components u_n and v_n for all values of n; but these approximations may not be accurate for some regions. For this reason, in this thesis, we construct a numerical method, Newton's method, which uses the VA as a starting point to find exact solutions. Newton's method is demonstrated and explained in [2]. Finding the exact solutions for the u_n and v_n components gives us the opportunity to compare the VA to the exact solutions and most importantly, pin-point the regions in which the VA gives a reasonable approximation to the exact solutions.

We have organized this paper as follows. In Chapter 2, we will describe the variational approximation. Then in Chapter 3, we will present the numerical method that will be used to obtain the exact solutions for u_n and v_n. The methodology for finding the exact solutions is presented in Chapter 4. In Chapter 5, we will discuss different possible exact solutions for different regions of existence and compare the VA solutions and exact solutions for three different cases. Lastly, in Chapter 6,

concluding remarks are made about our results; which include the regions for which the VA gives reasonable approximations to the exact solutions.

CHAPTER 2: THE VARIATIONAL APPROXIMATION

The VA is a tool which is well known for obtaining localized states in nonlinear systems. Once we have the VA solutions, we can proceed to use Newton's method to find exact solutions. In [11], the coupled DNLS equations for lattice fields ϕ_n and ψ_n is

$$i\frac{d}{dt}\phi_n = -\frac{1}{2}(\phi_{n+1} + \phi_{n-1} - 2\phi_n) - (|\phi_n|^2 + \beta|\psi_n|^2)\phi_n \ , \tag{2.1}$$

$$i\frac{d}{dt}\psi_n = -\frac{1}{2m}(\psi_{n+1} + \psi_{n-1} - 2\psi_n) - (|\psi_n|^2 + \beta|\phi_n|^2)\psi_n \ , \tag{2.2}$$

where $m > 0$ is the relative atomic mass of the two species in the case of BEC or the inverse ratio of the intersite coupling constants in the waveguide array, and $\beta < 0$ is the relative coefficient of the onsite cross-phase-modulation (XPM) coupling between the fields, while the coefficients of the self-phase modulation (SPM) nonlinearity for both fields are scaled to be 1. Solutions with unstaggered ϕ_n and staggered ψ_n onsite-centered components and two chemical potentials, λ and μ, are sought for as

$$\phi_n(t) = e^{-i\lambda t}u_n \ , \tag{2.3}$$

$$\psi_n(t) = e^{-i\mu t}(-1)^n v_n \ , \tag{2.4}$$

where ϕ_n and ψ_n are complex-valued functions for all integer values of the site index n. The eigenfunctions, u_n and v_n, are real values, which are also independent of time. They satisfy the following stationary equations:

$$(\lambda - 1)u_n + \frac{1}{2}(u_{n+1} + u_{n-1}) + (u_n^2 + \beta v_n^2)u_n = 0 \ , \tag{2.5}$$

$$(\mu - \frac{1}{m})v_n - \frac{1}{2m}(v_{n+1} + v_{n-1}) + (v_n^2 + \beta u_n^2)v_n = 0 \ . \tag{2.6}$$

These stationary equations can be derived from the Lagrangian,

$$L = \frac{1}{2}\sum_{n=-\infty}^{n=\infty}[-\frac{1}{2}(u_{n+1}-u_n)^2+\lambda u_n^2+\frac{1}{2m}(v_{n+1}-v_n)^2+(\mu-\frac{2}{m})v_n^2+\frac{1}{2}u_n^4+\frac{1}{2}v_n^4+\beta u_n^2 v_n^2] \ , \quad (2.7)$$

by taking the partial derivatives of L with respect to u_n and v_n.

Ref. [11] discussed an initial ansatz for solitons with unstaggered structures in both components, but here we focus on an initial ansatz for solitons with unstaggered structure in one component and twisted structure (spatially-antisymmetric) in the other component. The twisted component is negative for negative values of n, positive for positive values of n and zero for $n = 0$. In order to find soliton solutions, we utilize the exponential ansatz similar to the ones used in other models [1, 5, 6, 10]. This gives us approximations that decay exponentially as $|n|\to\infty$ as follows:

$$u_n = Ae^{-p|n|}, v_n = Bne^{-q|n|} \ . \quad (2.8)$$

Notice that the u_n and v_n components vanish exponentially as n increases.

A and B are the amplitudes of each component and are the variational parameters that are to be varied. The calculations for A and B are done in the following section. Notice that even though the v_n components of Eq. (2.8) do not satisfy the stationary equations, this is still a valid VA approximation. The n is multiplied to the B to keep $v_n < 0$ for $n < 0$ and $v_n > 0$ for $n > 0$, described by Figure 1.2. We can also find the decay rates of the waveforms of Eq. (2.8), p and q, from the linearized limit of Eqs. (2.5), (2.6) as $n \to \pm\infty$, which give us:

$$(\lambda - 1)u_n + \frac{1}{2}(u_{n+1} + u_{n-1}) = 0 \ , \quad (2.9)$$

$$(\mu - \frac{1}{m})v_n - \frac{1}{2m}(v_{n+1} + v_{n-1}) = 0 \ . \quad (2.10)$$

The solutions of Eq. (2.8) - Eq. (2.10) gives:

$$p = \ln[1 - \lambda + \sqrt{-\lambda(2-\lambda)}] \ , \tag{2.11}$$

$$q = \ln[m\mu - 1 + \sqrt{m\mu(m\mu-2)}] \ . \tag{2.12}$$

From the above, it follows that p and q to remain real and positive the ranges for λ and μ must be,

$$\lambda < 0, \mu > \frac{2}{m} \ . \tag{2.13}$$

Ref. [12] has also shown that solitons based on Eqs (2.8) exist and that we can obtain analytical approximations. For the rest of this paper, we will show that exact solutions can be found by using the numerical method constructed in Chapter 3. We will also demonstrate that depending on the values of A and B, the VA can be reasonably accurate compared to the exact solutions for both the u_n and v_n components.

Obtaining values of A^2 and B^2

By substituting Eqs (2.8) into the Lagrangian in Eq (2.7) and carrying out the summation, the following Lagrangian is produced:

$$\begin{aligned} L_{VA} = \frac{1}{2}(&-A^2 \tanh(\frac{p}{2}) + \lambda A^2 \coth(p) + \frac{A^4}{2}\coth(2p) + \frac{B^2}{2m}\frac{(\sinh(q))^{-1}}{\cosh(q)+1} \\ &+ \frac{B^2}{2}(\mu - \frac{2}{m})(\cosh^3(q) - \coth(q)) \\ &+ \frac{B^4}{2}[\frac{3}{2}\coth^5(2q) - \frac{5}{2}\coth^3(2q) + \coth(2q)] \\ &+ \frac{\beta A^2 B^2}{2}[\coth^3(p+q) - \coth(p+q)]) \end{aligned} \tag{2.14}$$

Taking the Lagrangian variables to be A^2 and B^2 gives rise to the following Euler-Lagrange equations:

$$\frac{\partial L_{VA}}{\partial(A^2)} = 0 \ , \tag{2.15}$$

$$\frac{\partial L_{VA}}{\partial(B^2)} = 0 \ . \tag{2.16}$$

By using Eq. (2.15), Eq. (2.16), and Eq. (2.14), we can achieve a system of linear equations to solve for A^2 and B^2. This system of equations is as follows:

$$[\coth(2p)]A^2 + \frac{\beta}{2}[\coth^3(p+q) - \coth(p+q)]B^2 = \tanh(\frac{p}{2}) - \lambda\coth(p) \ , \tag{2.17}$$

$$\begin{aligned}\frac{\beta}{2}[\coth^3(p+q) - \coth(p+q)]A^2 + [\frac{3}{2}\coth^5(2q) - \frac{5}{2}\coth^3(2q) + \coth(2q)]B^2 \\ = -\frac{1}{2m}\frac{\sinh(q)^{-1}}{\cosh(q)+1} - \frac{1}{2}(\mu - \frac{2}{m})(coth^3(q) - coth(q)) \ .\end{aligned} \tag{2.18}$$

Given these two equations, we can solve for A^2 and B^2. Meaningful physical solutions from the system of Eqs. (2.17) and (2.18), are given when $A^2 > 0$ and $B^2 > 0$. In the case A^2 or $B^2 < 0$, there are no solutions. In [12], it is shown that the existence of positive real solutions of A^2 and B^2 are present only when $\beta < 0$ and $m > 0$.

From Eq. (2.17) and Eq. (2.18), we can see that the values for A^2 and B^2 depend on λ and μ since p and q also depend on λ and μ. For the continuation of this thesis, we use $\beta = -5$, $m = 1$ and select different values of λ and μ. Given these values, we analyze how the VA solutions differ from the exact solutions for both the u_n and v_n components.

CHAPTER 3: CONSTRUCTING EXACT SOLUTIONS

Creation of the System of Equations

When constructing the convergence method for the exact solutions for the SUTS components, one must also remember that the VA are not exact solutions, they are usually a good approximation at which we can start our numerical method. In addition, the VA does not satisfy the stationary equations given by Eq. (2.5) and Eq. (2.6) and in order to satisfy these equations, we must vary the initial ansatz in Eq. (2.8) by slightly shifting the u_n and v_n components until we obtain that the magnitude of the stationary equations are less than 10^{-7}.

To begin, we let the stationary equations, Eq. (2.5) and Eq. (2.6), be designated by E_n and F_n, respectively. These equations have each value of u_n and v_n equal to the initial ansatz, $Ae^{-p|n|}$ and $Bne^{-q|n|}$, respectively. The shifts of E_n and F_n, which result from shifting the u_n and v_n components, are represented by δE_n and δF_n, respectively. These shifts are necessary because the VA does not satisfy the stationary equations exactly and adding or subtracting from these initial guesses will get us closer to the exact solutions. The shifting of the initial values of E_n and F_n are represented by the equations below:

$$E_n + \delta E_n = 0 \ , \tag{3.1}$$

$$F_n + \delta F_n = 0 \ . \tag{3.2}$$

Since the u_n components in Eq (2.8) are straight unstaggered, we have $u_{-1} = u_1$ whenever this is encountered. Similarly, since the v_n components in Eq. (2.8) are twisted, $v_0 = 0$ and $v_{-n} = -v_n$. Since the exact solutions involve an infinite number of values for n, we will limit the n by taking

$n \leq N$ where N is the value for which both $u_N, v_N \leq 10^{-12}$. This is possible since both u_n and $|v_n| \to 0$ exponentially as $n \to \infty$. Also, due to the symmetry of both the u_n and v_n components, we only need to consider positive values for n.

Below, are all of the values for E_n for $0 \leq n \leq N$:

$$E_0 = u_1 + (\lambda - 1)u_0 + u_0^3 \ , \tag{3.3}$$

$$E_1 = \frac{1}{2}u_2 + \frac{1}{2}u_0 + (\lambda - 1)u_1 + \beta v_1^2 u_1 + u_1^3 \ , \tag{3.4}$$

$$E_2 = \frac{1}{2}u_3 + \frac{1}{2}u_1 + (\lambda - 1)u_2 + \beta v_2^2 u_2 + u_2^3 \ , \tag{3.5}$$

$$\vdots$$

$$E_N = \frac{1}{2}u_{N+1} + \frac{1}{2}u_{N-1} + (\lambda - 1)u_N + \beta v_N^2 u_N + u_N^3 \quad . \tag{3.6}$$

Similarly, are all of the values for F_n for $0 \leq n \leq N$

$$F_0 = 0 \ , \tag{3.7}$$

$$F_1 = -\frac{1}{2m}v_2 + (\mu - \frac{1}{m})v_1 + v_1^3 + \beta u_1^2 v_1 \ , \tag{3.8}$$

$$F_2 = -\frac{1}{2m}v_1 - \frac{1}{2m}v_3 + (\mu - \frac{1}{m})v_2 + v_2^3 + \beta u_2^2 v_2 \ , \tag{3.9}$$

$$\vdots$$

$$F_N = -\frac{1}{2m}v_{N-1} - \frac{1}{2m}v_{N+1} + (\mu - \frac{1}{m})v_N + v_N^3 + \beta u_N^2 v_N \quad . \tag{3.10}$$

To find the δE_n and δF_n in Eq. (3.1) and Eq (3.2) for $0 \leq n \leq N$, we take the variations of E_n and F_n by varying u_n and v_n, respectively. We will also only consider the first order variations for

both the u_n and v_n components. This will give us the following results:

$$\delta E_0 = \delta u_1 + (\lambda - 1 + 3u_0^2)\delta u_0 \ , \tag{3.11}$$

$$\delta E_1 = \frac{1}{2}\delta u_2 + \frac{1}{2}\delta u_0 + (\lambda - 1 + \beta v_1^2 + 3u_1^2)\delta u_1 + 2\beta v_1 u_1 \delta v_1 \ , \tag{3.12}$$

$$\delta E_2 = \frac{1}{2}\delta u_3 + \frac{1}{2}\delta u_1 + (\lambda - 1 + \beta v_2^2 + 3u_2^2)\delta u_2 + 2\beta v_2 u_2 \delta v_2 \ , \tag{3.13}$$

$$\vdots$$

$$\delta E_N = \frac{1}{2}\delta u_{N+1} + \frac{1}{2}\delta u_{N-1} + (\lambda - 1 + \beta v_N^2 + 3u_N^2)\delta u_N + 2\beta v_N u_N \delta v_N \quad , \tag{3.14}$$

$$\delta F_0 = 0 \ , \tag{3.15}$$

$$\delta F_1 = -\frac{1}{2m}\delta v_2 + (\mu - \frac{1}{m} + 3v_1^2 + \beta u_1^2)\delta v_1 + 2\beta u_1 v_1 \delta u_1 \ , \tag{3.16}$$

$$\delta F_2 = -\frac{1}{2m}\delta v_1 - \frac{1}{2m}\delta v_3 + (\mu - \frac{1}{m} + 3v_2^2 + \beta u_2^2)\delta v_2 + 2\beta u_2 v_2 \delta u_2 \ , \tag{3.17}$$

$$\vdots$$

$$\delta F_N = -\frac{1}{2m}\delta v_{N-1} - \frac{1}{2m}\delta v_{N+1} + (\mu - \frac{1}{m} + 3v_N^2 + \beta u_N^2)\delta v_N + 2\beta u_N v_N \delta u_N \quad . \tag{3.18}$$

Now that we have calculated the values for E_n, δE_n, F_n and δF_n, we can demonstrate the process of how to construct the matrix by using the first couple of equations: E_0, δE_0, F_1, and δF_1. Substituting E_0, δE_0, F_1, and δF_1 into Eq. (3.1) and Eq. (3.2), will get us the following equations.

$$E_0 + \delta E_0 = u_1 + (\lambda - 1)u_0 + u_0^3 + \delta u_1 + (\lambda - 1 + 3u_0^2)\delta u_0 = 0 \ , \tag{3.19}$$

$$F_1 + \delta F_1 = (\mu - \frac{1}{m})v_1 + v_1^3 + \beta u_1^2 v_1 + (\mu - \frac{1}{m} + 3v_1^2 + \beta u_1^2)\delta v_1 - \frac{1}{2m}v_2 - \frac{1}{2m}\delta v_2 + 2\beta u_1 v_1 \delta u_1 = 0 \ . \tag{3.20}$$

Since the first couple of terms in the above equations are known, the first part of these equations become numerical values. On the other hand, the last part of the equations are not known because the δu_n and δv_n for $0 \leq n \leq N$ are unknown. Therefore, to satisfy Eq. (3.1) and Eq (3.2), we must solve the above equations for the values of δu_n and δv_n. When doing this, we achieve a set of equations of size $N+1$ for E_n and size N for F_n. The following sections will explain how to construct the matrices necessary to calculate δu_n and δv_n.

Construction of the Block Matrix

Since we have $N+1$ unknowns for E_n and N unknowns for F_n, we can construct an $(N+1)$ by (N) matrix to solve for the values of δu_n and δv_n. From Eq. (3.1) to Eq. (3.16), we are able to construct the following tri-diagonal matrix, TDV. In TDV, each column represents the coefficient attached to the δv_n, for $1 \leq n \leq N$. Notice that the δF_n equations also have δu_n values; these values will be represented using the diagonal matrix DV. In the matrix DV, the columns contain the coefficient of δu_n, for $0 \leq n \leq N$. Notice that the first row of each matrix TDV and DV consist of the δv_n and δu_n values given in Eq. (3.20), respectively.

.

$$TDV = \begin{vmatrix} (\mu - \frac{1}{m} + 3v_1^2 + \beta u_1^2) & -\frac{1}{2m} & 0 & 0 \ldots & 0 & 0 & 0 \\ -\frac{1}{2m} & (\mu - \frac{1}{m} + 3v_2^2 + \beta u_2^2) & -\frac{1}{2m} & 0 \ldots & 0 & 0 & 0 \\ . & . & . & . \ldots & . & . & . \\ . & . & . & . \ldots & . & . & . \\ . & . & . & . \ldots & . & . & . \\ 0 & 0 & 0 & 0 \ldots & -\frac{1}{2m} & (\mu - \frac{1}{m} + 3v_{N-1}^2 + \beta u_{N-1}^2) & -\frac{1}{2m} \\ 0 & 0 & 0 & 0 \ldots & 0 & -\frac{1}{2m} & (\mu - \frac{1}{m} + 3v_N^2 + \beta u_N^2) \end{vmatrix}.$$

$$DV = \begin{vmatrix} 0 & 2\beta u_1 v_1 & 0 & 0 & \ldots & 0 & 0 \\ 0 & 0 & 2\beta u_2 v_2 & 0 & \ldots & 0 & 0 \\ 0 & 0 & 0 & 2\beta u_3 v_3 & \ldots & 0 & 0 \\ . & . & . & . & \ldots & . & . \\ . & . & . & . & \ldots & . & . \\ . & . & . & . & \ldots & . & . \\ . & . & . & . & \ldots & 2\beta u_{N-1} v_{N-1} & 0 \\ 0 & 0 & 0 & 0 & \ldots & 0 & 2\beta u_N v_N \end{vmatrix}.$$

Notice that the value for δv_{N+1} cannot appear in the matrix TDV because the column which would have this value is not included in matrix TDV. The last δv_n value which is calculated from matrix TDV is δv_N. But we must calculate δv_{N+1} because this value is required to calculate the condition of $F_N + \delta F_N = 0$. Since we have the connection that $v_N = BNe^{-Nq}$ and

$v_{N+1} = B(N+1)e^{-(N+1)q}$, we can estimate the value of δv_{N+1} to be as follows:

$$\delta v_{N+1} = \frac{N+1}{N} e^{-q} \delta v_N \ . \tag{3.21}$$

Similarly, we can estimate δu_{N+1} as follows:

$$\delta u_{N+1} = e^{-p} \delta u_N \ . \tag{3.22}$$

We will create matrices TDU and DU, which represent δE_n, in a manner similar to how we constructed matrices TDV and DV. The code for the construction of matrices TDU and DU is given in the Appendix. After the four matrices are constructed, we will join them to create a block matrix of the following form:

$$MAT = \begin{vmatrix} TDU & DU \\ DV & TDV \end{vmatrix}.$$

MAT can now be used to represent the coefficients of the system of equations for δE_n and δF_n in Eq (3.1) and Eq (3.2). The column vector VecUV, shown below, contains each value of E_n for $0 \leq n \leq N$ and F_n for $1 \leq n \leq N$. Notice that since each E_n and F_n is a numerical value, each element of column vector $VecUV$ can be calculated. We must also create a column vector with each variable for δu_n and δv_n. This is represented by the column vector $Delu_n v_n$, shown below.

$$VecUV = \begin{vmatrix} E_0 \\ E_1 \\ E_2 \\ . \\ . \\ . \\ E_n \\ F_1 \\ F_2 \\ F_3 \\ . \\ . \\ . \\ F_n \end{vmatrix}, \; Delu_nv_n = \begin{vmatrix} \delta u_0 \\ \delta u_1 \\ \delta u_2 \\ . \\ . \\ . \\ \delta u_n \\ \delta v_1 \\ \delta v_2 \\ \delta v_3 \\ . \\ . \\ . \\ \delta v_n \end{vmatrix}$$

Finally, Eq (3.1) and Eq (3.2) now have the following matrix representation.

$$VecUV + (MAT) \cdot Delu_nv_n = 0 \tag{3.23}$$

CHAPTER 4: METHODOLOGY FOR FINDING THE EXACT SOLUTIONS

As in Newton's Method, one comes closer to the solution by iterating on the method. For that reason, solving for δu_n and δv_n, one time might not be enough to get the exact solutions that we are interested in achieving. Therefore, a simple algorithm to find the necessary exact solutions can be made by letting the following be the initial values for u_n and v_n:

$$u_{n_0} = Ae^{-p|n|}, v_{n_0} = Bne^{-q|n|} \ . \tag{4.1}$$

We then substitute these values, u_{n_0} and v_{n_0}, into Eq. (3.1) and Eq. (3.2) and solve for the δu_n and δv_n values, by using the steps described in Chapter 3, which will be defined as δu_{n_0} and δv_{n_0}, respectively. These delta values will be added to each u_{n_0} and v_{n_0}, which gives us the following values:

$$u_{n_1} = u_{n_0} + \delta u_{n_0}, v_{n_1} = v_{n_0} + \delta v_{n_0} \ . \tag{4.2}$$

These are the new values for u_n and v_n which should be closer to the exact solutions. These new values of u_n and v_n are again substituted into Eq. (3.23) to solve for the new set of δu_n and δv_n values. Iterating this process, gives us the general form for the u_n and v_n values:

$$u_{n_{k+1}} = u_{n_k} + \delta u_{n_k}, v_{n_{k+1}} = v_{n_k} + \delta v_{n_k} \qquad (k \geq 0). \tag{4.3}$$

Once we find the values of u_n and v_n that make Eq. (2.5) and Eq. (2.6) less than 10^{-7}, we can stop the iteration process and take these values of u_n and v_n as being the exact solutions.

Check for Convergence of Exact Solutions

After each iteration, we can substitute the values of u_n and v_n into Eq. (3.23), and evaluate each term of VecUV. Doing this, gives us the value of each stationary equation. Since we want the u_n and v_n values to satisfy the stationary equations, we would like to see each term of VecUV converging to zero. For this reason, we will take the norm of VecUV after every iteration and make sure that this value is decreasing. Fortunately, the initial guess, using the VA, has been adequate and the norm of VecUV always decreases. As a consequence of the norm of VecUV decreasing, each element of VecUV is also decreasing, which means that each stationary equation is converging to zero. This process is stopped when each element of column vector $VecUV$ has decreased to be less than 10^{-7}, which is the definition for exact solutions.

CHAPTER 5: COMPARING THE VA AND EXACT SOLUTIONS

Existence Regions for VA and Exact Solutions

In this chapter we will search for regions of existence for both the VA and exact solutions. Finding these regions will allow us to analyze the different behaviors of the u_n and v_n components. Pinpointing different regions of existence will also help us find the regions in which the VA and exact solutions are the most similar and diverse. In order to find the existence regions for both the VA and exact solutions, we must solve the system of equations, Eq. (2.17) and Eq. (2.18) for A^2 and B^2. Solving these equations show us that there are existence and nonexistence regions that depend on λ and μ. From [12], using $m = 1, \beta = -5$, the range of λ is $[-0.6, 0)$ and the range of μ is $(2.0, 3.0]$, we achieve the following figure.

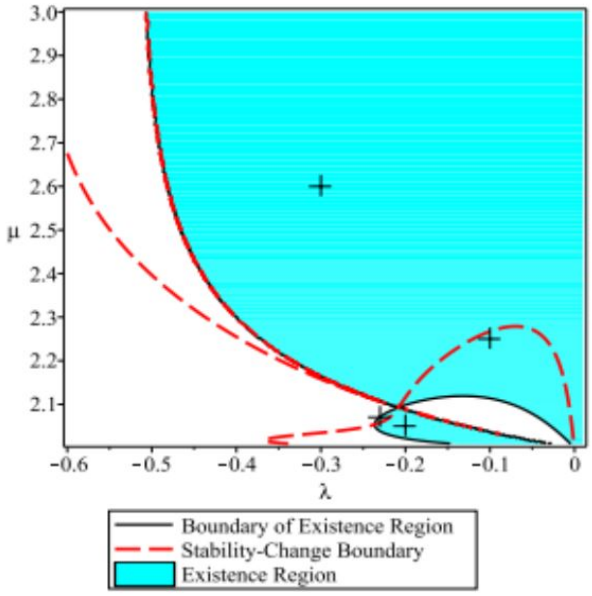

Figure 5.1: This plot is constructed in [12]. We do not consider the stability-change boundary in this thesis. Existence regions predicted by the VA for the discrete solitons with SUTS components, with ansatz described by Eq. (2.8), and $m = 1$, $\beta = -5$. The existence region for solutions, $A^2 > 0$ and $B^2 > 0$ is shaded in blue. There are four existence regions. Solitons from each of these regions corresponds to the + symbols.

Results for the VA and the Exact Solutions

From Figure 5.1, we can see that there are four regions of possible VA solutions. Since we need the VA for an initial guess to calculate the exact solutions, we will also have four different regions for exact solutions. As a result, exact solutions may demonstrate different results for the u_n and v_n components depending on the region that there are located in. To test this, we will take one point from each existence region and analyze the SUTS soliton solutions for both the VA and the exact solutions. The following figure demonstrates the results of the four points, (λ, μ), using the VA.

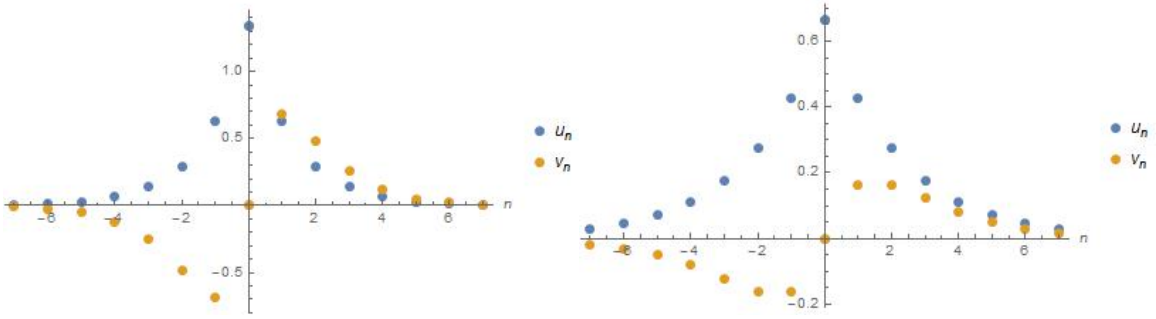

(a) $\lambda = -0.3, \mu = 2.6$

(b) $\lambda = -0.1, \mu = 2.25$

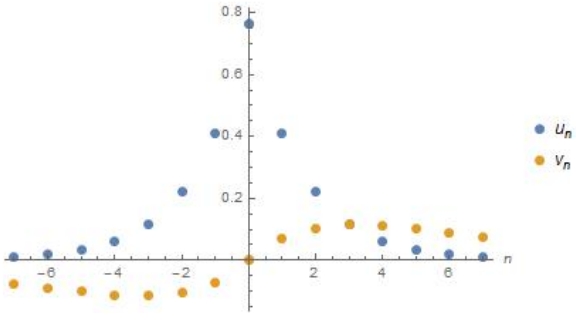

(c) $\lambda = -0.2, \mu = 2.05$

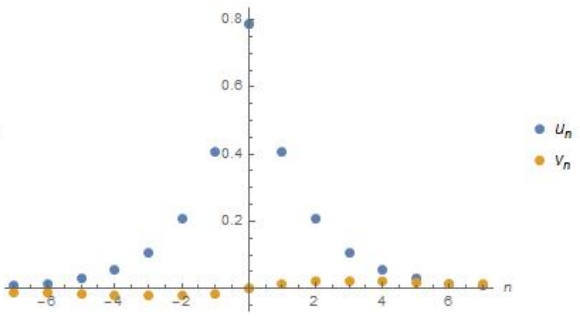

(d) $\lambda = -0.23, \mu = 2.07$

Figure 5.2: Shapes of the discrete solitons with the SUTS components, with initial ansatz, Eq. (2.8), using VA.

To make comparisons between the VA and the exact solutions, we will use the same four points used to calculate the VA, to calculate the exact solutions. Here is where we will make use of the numerical method constructed in Chapter 3 and the methodology outlined in Chapter 4.

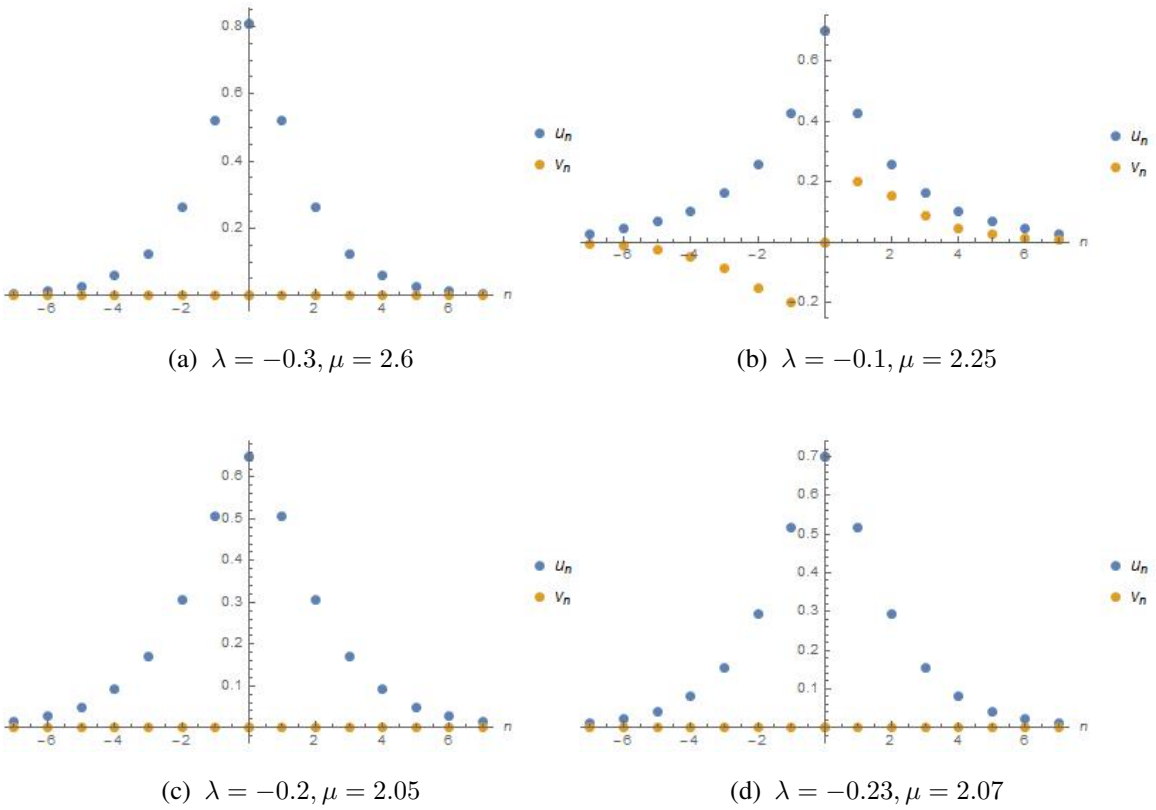

(a) $\lambda = -0.3, \mu = 2.6$ (b) $\lambda = -0.1, \mu = 2.25$

(c) $\lambda = -0.2, \mu = 2.05$ (d) $\lambda = -0.23, \mu = 2.07$

Figure 5.3: Shapes of the Exact Solutions for the discrete solitons with the SUTS components, with initial ansatz Eq. (2.8).

Using the methodology in Chapter 4 will show us how the δu_n and δv_n, of each of the four points, (λ,μ), decrease to zero. This is exactly what we wish to see happening because this means that the values of u_n and v_n are converging to the exact solutions. After a few iterations, we achieve the exact solutions in Figure 5.2.

Notice that for the exact solutions achieved above, three of the four points, (λ, μ), have the v_n components equal to zero for all values of n; whereas the VA solutions have both u_n and $|v_n|$ components greater than zero. A detailed comparison of these four points, (λ,μ), is given in the

following section.

Comparisons

One would expect for the exact solutions to be different from the VA solutions since the VA solutions were used as starting points to find the exact solutions. Since differences are expected, we will graphically and numerically compare the exact and VA solutions for the four points (λ, μ) plotted in Figures 5.2 and 5.3.

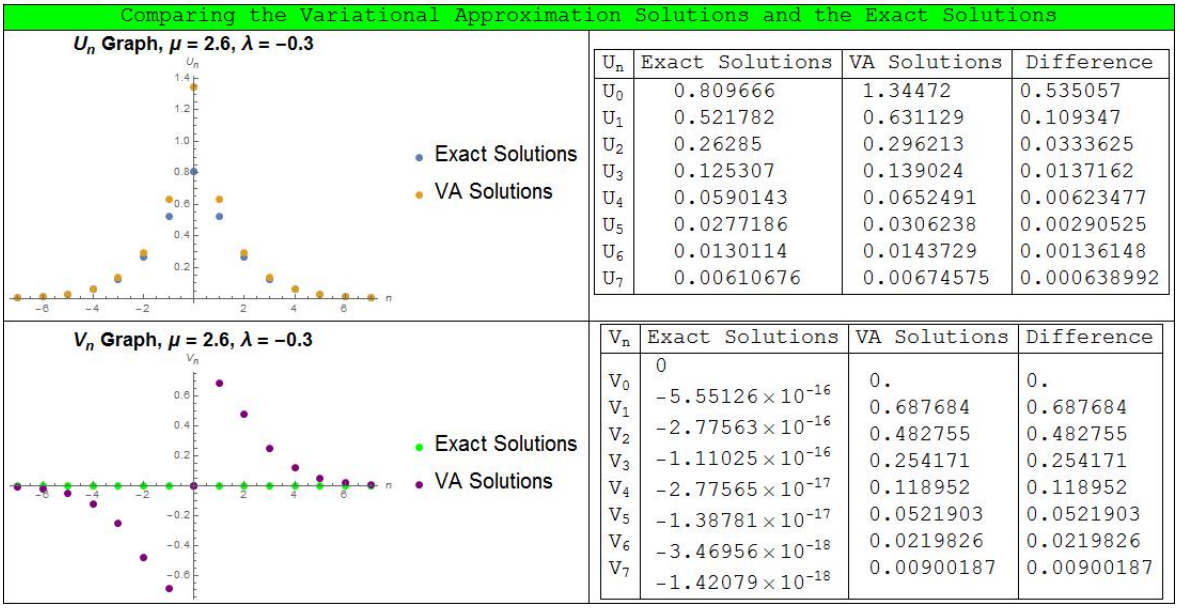

U_n	Exact Solutions	VA Solutions	Difference
U_0	0.809666	1.34472	0.535057
U_1	0.521782	0.631129	0.109347
U_2	0.26285	0.296213	0.0333625
U_3	0.125307	0.139024	0.0137162
U_4	0.0590143	0.0652491	0.00623477
U_5	0.0277186	0.0306238	0.00290525
U_6	0.0130114	0.0143729	0.00136148
U_7	0.00610676	0.00674575	0.000638992

V_n	Exact Solutions	VA Solutions	Difference
V_0	0	0.	0.
V_1	-5.55126×10^{-16}	0.687684	0.687684
V_2	-2.77563×10^{-16}	0.482755	0.482755
V_3	-1.11025×10^{-16}	0.254171	0.254171
V_4	-2.77565×10^{-17}	0.118952	0.118952
V_5	-1.38781×10^{-17}	0.0521903	0.0521903
V_6	-3.46956×10^{-18}	0.0219826	0.0219826
V_7	-1.42079×10^{-18}	0.00900187	0.00900187

Figure 5.4: Comparison of Figure 5.2 part (a) and Figure 5.3 part (a) for the SUTS discrete solitons, with $m = 1$ and $\beta = -5$. We plot the u_n values for both the exact and the VA solutions on the top part and the v_n values for both the exact and the VA solutions on the bottom part of the figure. While the shape for the u_n components for the exact and VA solutions are similar, the v_n are very different. According to the exact solutions, the values for v_n are zero.

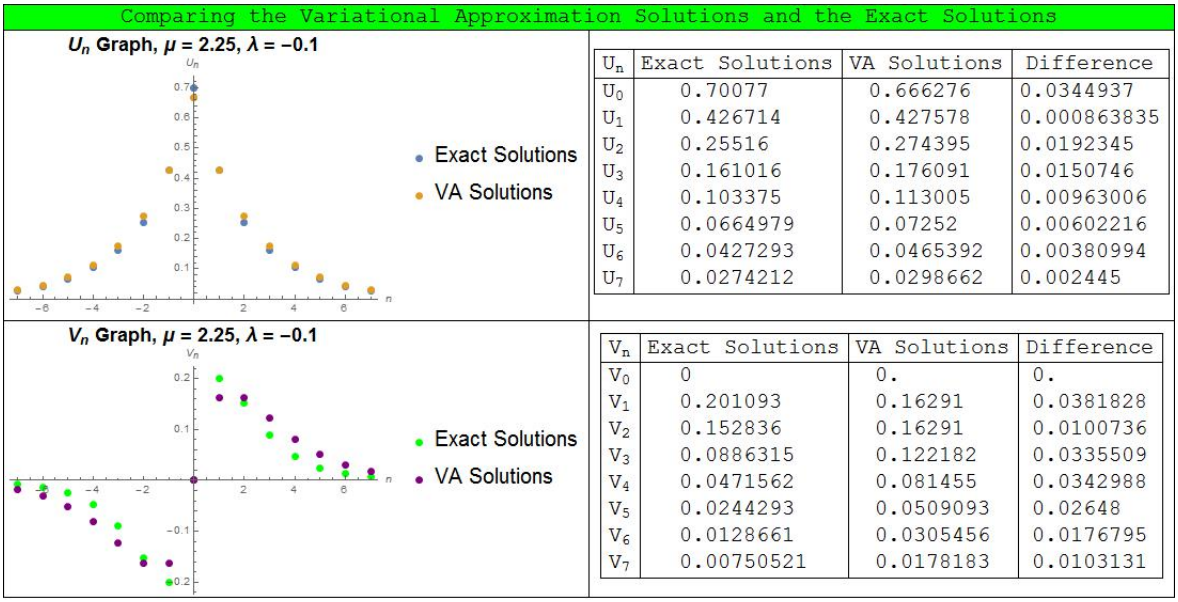

U_n	Exact Solutions	VA Solutions	Difference
U_0	0.70077	0.666276	0.0344937
U_1	0.426714	0.427578	0.000863835
U_2	0.25516	0.274395	0.0192345
U_3	0.161016	0.176091	0.0150746
U_4	0.103375	0.113005	0.00963006
U_5	0.0664979	0.07252	0.00602216
U_6	0.0427293	0.0465392	0.00380994
U_7	0.0274212	0.0298662	0.002445

V_n	Exact Solutions	VA Solutions	Difference
V_0	0	0.	0.
V_1	0.201093	0.16291	0.0381828
V_2	0.152836	0.16291	0.0100736
V_3	0.0886315	0.122182	0.0335509
V_4	0.0471562	0.081455	0.0342988
V_5	0.0244293	0.0509093	0.02648
V_6	0.0128661	0.0305456	0.0176795
V_7	0.00750521	0.0178183	0.0103131

Figure 5.5: Comparison of Figure 5.2 part (b) and Figure 5.3 part (b) for the SUTS discrete solitons, with $m = 1$ and $\beta = -5$. We plot the u_n values for both the exact and the VA solutions on the top part and the v_n values for both the exact and the VA solutions on the bottom part of the figure. For these values of μ and λ the shape for the exact solution and the VA solutions for both the u_n and v_n components are similar. Furthermore, this implies that the VA gives an accurate approximation to the exact solution at point, $(\lambda = -0.1, \mu = -2.25)$.

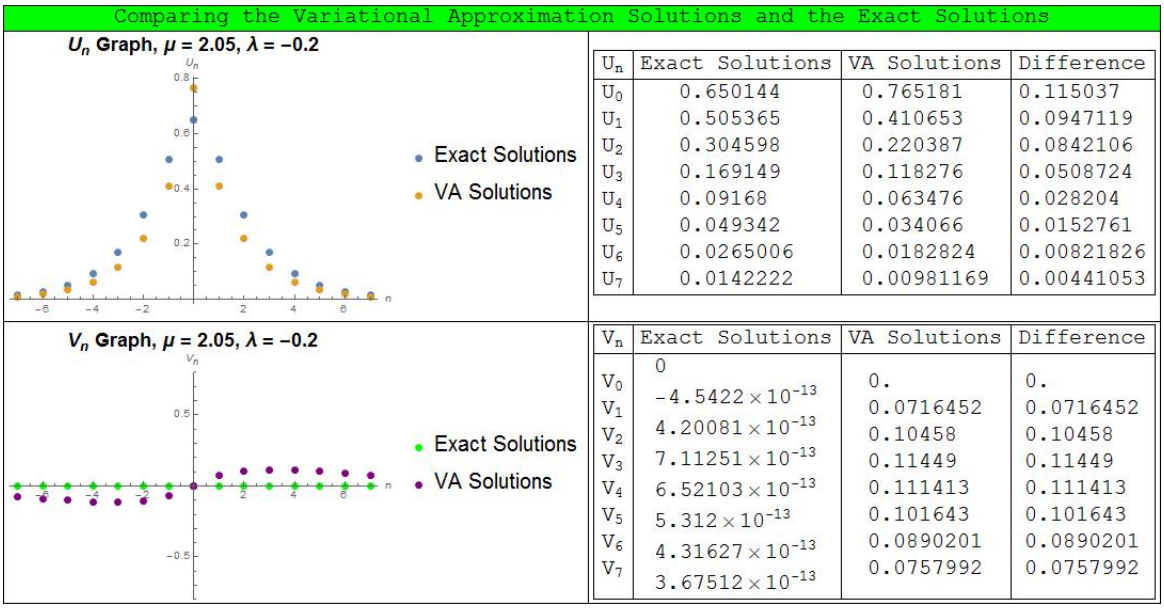

U_n	Exact Solutions	VA Solutions	Difference
U_0	0.650144	0.765181	0.115037
U_1	0.505365	0.410653	0.0947119
U_2	0.304598	0.220387	0.0842106
U_3	0.169149	0.118276	0.0508724
U_4	0.09168	0.063476	0.028204
U_5	0.049342	0.034066	0.0152761
U_6	0.0265006	0.0182824	0.00821826
U_7	0.0142222	0.00981169	0.00441053

V_n	Exact Solutions	VA Solutions	Difference
V_0	0	0.	0.
V_1	-4.5422×10^{-13}	0.0716452	0.0716452
V_2	4.20081×10^{-13}	0.10458	0.10458
V_3	7.11251×10^{-13}	0.11449	0.11449
V_4	6.52103×10^{-13}	0.111413	0.111413
V_5	5.312×10^{-13}	0.101643	0.101643
V_6	4.31627×10^{-13}	0.0890201	0.0890201
V_7	3.67512×10^{-13}	0.0757992	0.0757992

Figure 5.6: Comparison of Figure 5.2 part (c) and Figure 5.3 part (c) for the SUTS discrete solitons, with $m = 1$ and $\beta = -5$. We plot the u_n values for both the exact and the VA solutions on the top part and the v_n values for both the exact and the VA solutions on the bottom part of the figure. The shapes for the u_n and v_n components for the exact and VA solutions are similar. According to the exact solutions, the values for the v_n components are zero. This means that the exact solution does not have a twisted staggered component.

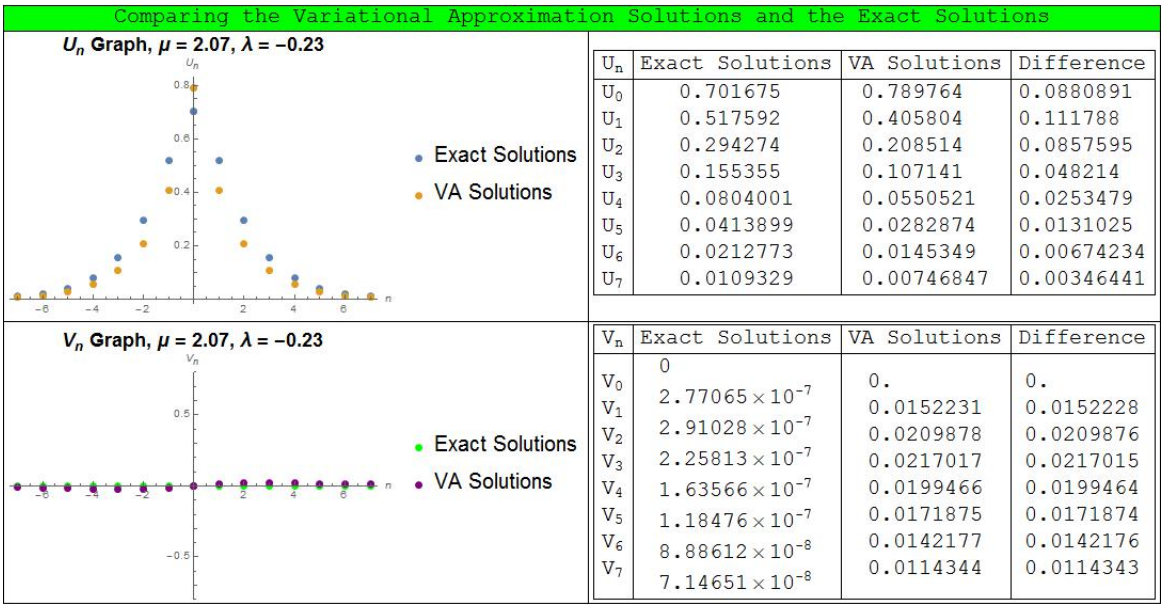

U_n	Exact Solutions	VA Solutions	Difference
U_0	0.701675	0.789764	0.0880891
U_1	0.517592	0.405804	0.111788
U_2	0.294274	0.208514	0.0857595
U_3	0.155355	0.107141	0.048214
U_4	0.0804001	0.0550521	0.0253479
U_5	0.0413899	0.0282874	0.0131025
U_6	0.0212773	0.0145349	0.00674234
U_7	0.0109329	0.00746847	0.00346441

V_n	Exact Solutions	VA Solutions	Difference
V_0	0	0.	0.
V_1	2.77065×10^{-7}	0.0152231	0.0152228
V_2	2.91028×10^{-7}	0.0209878	0.0209876
V_3	2.25813×10^{-7}	0.0217017	0.0217015
V_4	1.63566×10^{-7}	0.0199466	0.0199464
V_5	1.18476×10^{-7}	0.0171875	0.0171874
V_6	8.88612×10^{-8}	0.0142177	0.0142176
V_7	7.14651×10^{-8}	0.0114344	0.0114343

Figure 5.7: Comparison of Figure 5.2 part (d) and Figure 5.3 part (d) for the SUTS discrete solitons, with $m = 1$ and $\beta = -5$. We plot the u_n values for both the exact and the VA solutions on the top part and the v_n values for both the exact and the VA solutions on the bottom part of the figure. The shapes for the u_n and v_n components for the exact and VA solutions are very similar. According to the exact solutions, the values for the v_n components are zero and the VA predicts the v_n components to be close to zero .

Since the only difference that these four figures have is the value of λ and μ, we can suggest that the accuracy at which the VA predicts the exact solutions is based on specific regions of existence. After comparing the four points which lay in the four different regions of existence, we can say that the VA estimates the last three points, $(\lambda = -0.1, \mu = -2.25)$, $(\lambda = -0.2, \mu = -2.05)$ and $(\lambda = -0.23, \mu = -2.07)$, fairly well; but the first point, $(\lambda = -0.3, \mu = -2.6)$, not too well. In the following sections, we will see that a slight change in λ or μ can have a large effect on how well the VA predicts the exact solution.

Existence Regions for Exact Solutions

With the exact solutions that we have achieved in the last section, we have noticed that there are three scenarios that can occur:

1). Both u_n and v_n values exist and are nonzero.

2). The u_n values are nonzero and the v_n values zero.

3). The u_n values are zero and the v_n values are nonzero.

It would be interesting to see if there are specific regions that give the three scenarios described above, so we will analyze Figure 5.1 in more detail. In the following subsections, we will present the figures which represent the regions for the three scenarios described above. We will find that some of the points, (λ,μ), used in the comparisons of the last section were close to the border of two different regions of existence.

$$u_n, v_n > 0$$

By running the method described in Chapter 4, we will find the exact solutions for all points and determine if the u_n and v_n components are both greater than zero. According to Figure 5.3, point ($\lambda = -0.1, \mu = 2.25$) has this solution.

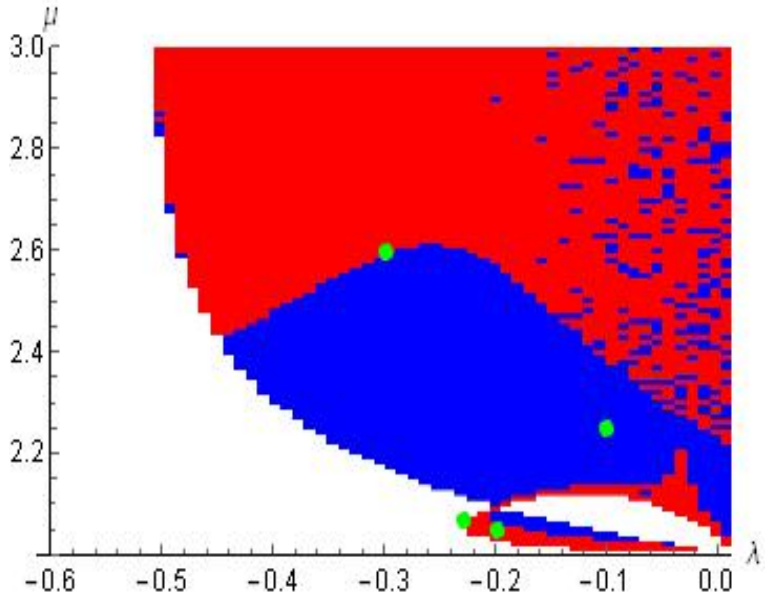

Figure 5.8: Existence regions predicted by the exact solutions for the discrete solitons with SUTS components, with ansatz described by Eq. (2.8) where the values of $A^2, B^2 > 0$ and $m = 1$, $\beta = -5$. The existence regions for solutions $u_n > 0$ and $v_n > 0$ are shaded in blue and the regions shaded in red are other solutions that exist, but are not $u_n > 0$ and $v_n > 0$. Points of interest are dotted in green.

Notice that point $(\lambda = -0.1, \mu = 2.25)$, which is Figure 5.5, lays in the blue region of Figure 5.8. In Figure 5.5, the VA solutions and the exact solutions for point $(\lambda = -0.1, \mu = 2.25)$ are very close in both the u_n and the v_n components. This is because the values of A^2 and B^2 are both greater than zero for the VA, and the exact solutions also lay in a region that has both the u_n and the v_n components greater than zero. We could say that the initial guess to calculate the exact solution is accurate for this point. In addition, Figure 5.8 indicates that besides the large blue region in which point $(\lambda = -0.1, \mu = 2.25)$ lays, there is another region in which exact solutions also have both the u_n and v_n components greater than zero. An example of this is the small blue region above point $(\lambda = -0.2, \mu = 2.05)$.

Taking a point from this region, for instance $(\lambda = -0.2, \mu = 2.06)$, will show us similar accuracy in the predictions made by the VA for the exact solutions. Figure 5.9, demonstrates this for both the u_n and v_n components. Even though the v_n components for the exact solution are greater than the VA for the first couple of values of n, we can see that after v_3, their difference is much smaller and the VA approximates the exact solutions quite well.

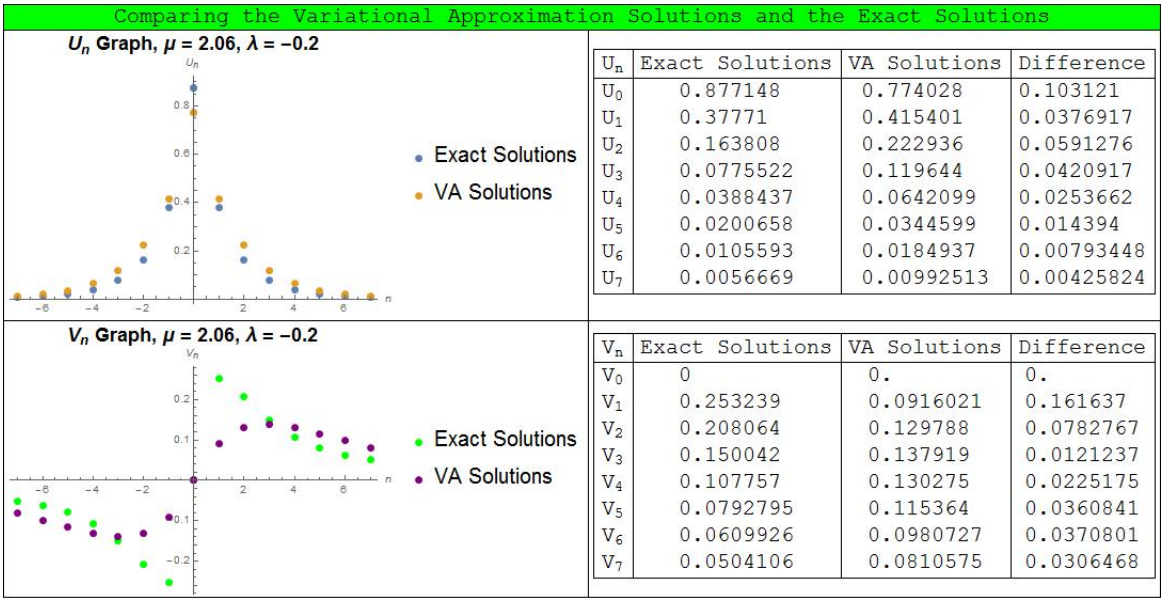

U_n	Exact Solutions	VA Solutions	Difference
U_0	0.877148	0.774028	0.103121
U_1	0.37771	0.415401	0.0376917
U_2	0.163808	0.222936	0.0591276
U_3	0.0775522	0.119644	0.0420917
U_4	0.0388437	0.0642099	0.0253662
U_5	0.0200658	0.0344599	0.014394
U_6	0.0105593	0.0184937	0.00793448
U_7	0.0056669	0.00992513	0.00425824

V_n	Exact Solutions	VA Solutions	Difference
V_0	0	0.	0.
V_1	0.253239	0.0916021	0.161637
V_2	0.208064	0.129788	0.0782767
V_3	0.150042	0.137919	0.0121237
V_4	0.107757	0.130275	0.0225175
V_5	0.0792795	0.115364	0.0360841
V_6	0.0609926	0.0980727	0.0370801
V_7	0.0504106	0.0810575	0.0306468

Figure 5.9: Comparison of the exact solutions and VA using $(\lambda = -0.2, \mu = 2.06)$. According to Figure 5.8, the values for both the u_n and v_n components would be greater than zero and this is exactly what we see from the figures and tables above.

If we analyze other points in the blue regions of Figure 5.8 we will also get similar exact solutions for the u_n and v_n components. But if we slightly change the value of μ to be equal to 2.05, instead

of 2.06, we will observe completely different exact solutions. The solutions obtained for point, $(\lambda = -0.2, \mu = 2.05)$, are discussed in the following section.

$$u_n > 0, v_n = 0 \textit{ and } u_n = 0, v_n > 0$$

From the results that we obtained in Figure 5.3 parts (a), (c), (d), we can see that the exact solutions for the v_n components equal zero while the values of the u_n components are nonzero. Having all of the v_n components equal to zero indicates that the amplitude of the initial ansatz, Eq. (2.8), for the v_n components is also zero. For this reason, we will also determine the regions of paraments (λ, μ) that give us exact solutions of $v_n = 0$. The following figure shows us these regions shaded in blue.

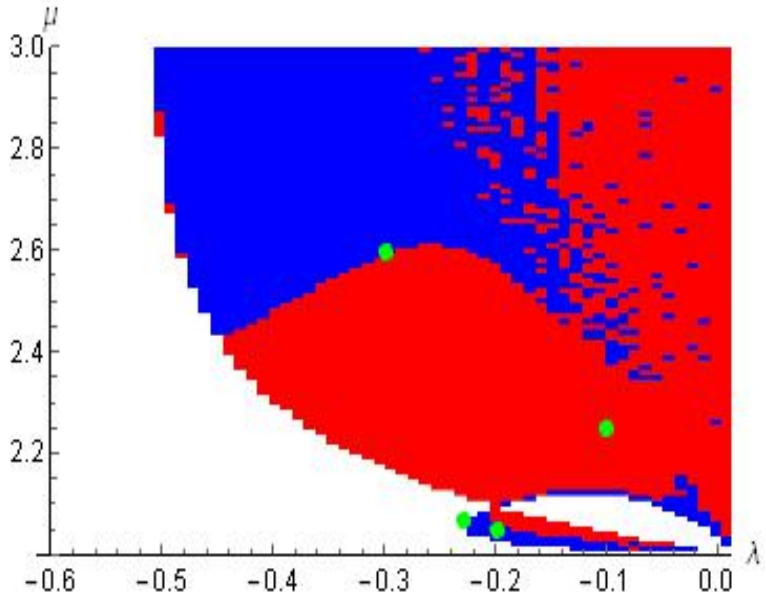

Figure 5.10: Existence regions predicted by the exact solutions for the discrete solitons with SUTS components, with ansatz described by Eq. (2.8) where the values of $A^2, B^2 > 0$ and $m = 1$, $\beta = -5$. The existence regions for solutions $u_n > 0$ and $v_n = 0$ are shaded in blue and the regions shaded in red are other solutions that exist, but are not $u_n > 0$ and $v_n = 0$. Points of interest are dotted in green.

Figure 5.10 indicates that points $(\lambda = -0.3, \mu = 2.6)$, $(\lambda = -0.2, \mu = 2.05)$ and $(\lambda = -0.23, \mu = 2.07)$ are all on the blue regions which correctly predicts the behaviors of the v_n components seen in Figure 5.3 parts (a), (b), (c). Furthermore, if we force the value of $B = 0$ in the VA, we will see the accuracy of which the VA estimates the solitons to the exact solutions. The only problem is that forcing $B = 0$, will not give us the shaded regions in Figure 5.10 because Figure 5.10 only has the regions of existence given A^2 and $B^2 > 0$. Therefore, if we set $B^2 = 0$, we will not get a VA approximation for points $(\lambda = -0.3, \mu = 2.6)$, $(\lambda = -0.2, \mu = 2.05)$, and $(\lambda = -0.23, \mu = 2.07)$ and instead get points with other values of λ and μ.

To fully test the results that are given by Figure 5.10, we will use point $(\lambda = -0.3, \mu = 2.59)$, which is not in the blue region of Figure 5.10, to show that the v_n components of the exact solutions do not converge to zero. Note that point $(\lambda = -0.3, \mu = 2.59)$ is very close to point $(\lambda = -0.3, \mu = 2.6)$, which lays in the blue shaded region of Figure 5.10. The exact solutions for both the u_n and v_n components for point $(\lambda = -0.3, \mu = 2.59)$ are plotted in Figure 5.11. Figure 5.11 shows us that all of the v_n components are not equal to zero. Even though the values for the v_n components at point $(\lambda = -0.3, \mu = 2.59)$ are small, we still obtain the twisted staggered characteristic unlike point $(\lambda = -0.3, \mu = 2.6)$. Once again, these two points are an example that demonstrate that the slightest change in μ can cause a significant difference in exact solutions.

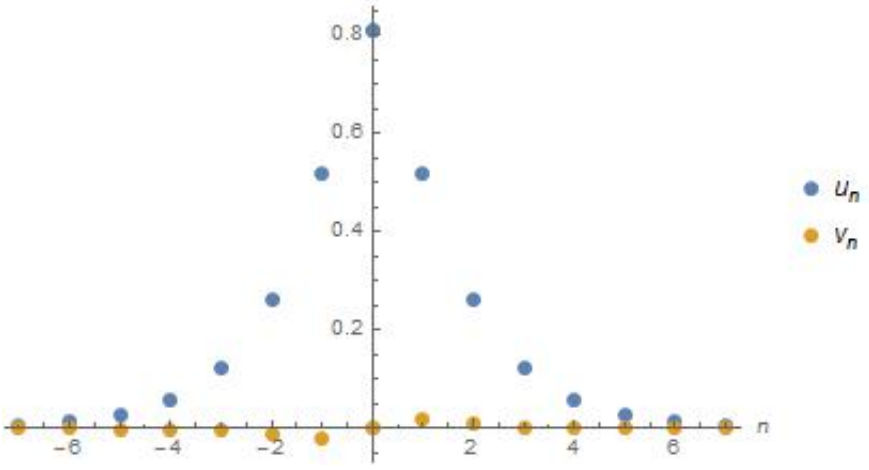

Figure 5.11: Shapes of the Exact Solutions for the discrete solitons with the SUTS components, with initial ansatz Eq. (2.8) using $(\lambda = -0.3, \mu = 2.59)$.

Since the combinations of the first two scenarios gave us such interesting results and significant insights about the exact solutions, we decided to also investigate the situation of when the exact solutions give $u_n = 0$ and $v_n > 0$ for all components. But after running the methodology discussed

in chapter 4, we found that the regions of where these exact solutions exist are actually not found. According to Figure 5.12, there are no parameters of λ and μ that give these solutions.

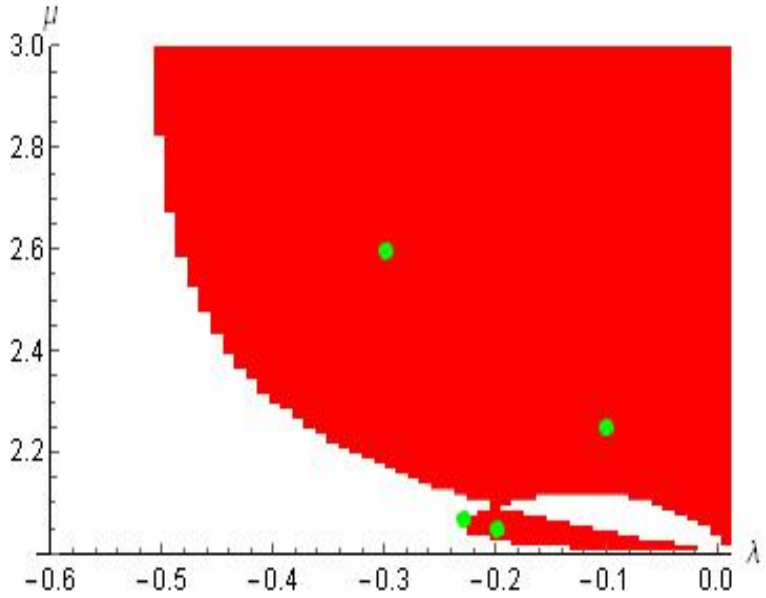

Figure 5.12: Existence regions predicted by the exact solutions for the discrete solitons with SUTS components, with ansatz described by Eq. (2.8) where the values of $A^2, B^2 > 0$ and $m = 1$, $\beta = -5$. The existence region for solutions $u_n = 0$ and $v_n > 0$ is the region shaded in blue and the region shaded in red are other solutions that exist, but are not $u_n = 0$ and $v_n > 0$. Points of interest are dotted in green.

CHAPTER 6: CONCLUSION

After completing the analysis and comparison of the VA solutions and exact solutions of the SUTS discrete solitons, we were able to gather interesting results about certain regions of existence. With these regions, we were able to conclude that the overall accuracy done by the VA for both of the u_n and v_n components is dependent on the exact solutions for the v_n components. For every point that we observed, we noticed that the VA approximates the u_n components of the soliton extremely well. We have found that exact solutions that have v_n components equal to zero are not approximated well by the VA. On the other hand, we also found that when the exact solutions for both of the u_n and v_n components are greater than zero, the VA approximates both of the u_n and the v_n components very accurately; specially if the points are not near existence region borders. Lastly, we were not able to find any existence regions which had exact solutions for the u_n components equal to zero and the v_n components greater than zero.

For further research, we would like to analyze exact solutions given by the VA that have $A^2 > 0$ and $B^2 = 0$, and $A^2 = 0$ and $B^2 > 0$. It would be interesting to see if the points that lay in these regions also have exact solutions with $u_n > 0$ and $v_n = 0$, and $u_n = 0$ and $v_n > 0$, respectively.

APPENDIX : MATHEMATICA CODE

Using Mathematica, the code below is used to construct matrices TDU and DU, which are discussed in chapter 3.

```
TDU = SparseArray[{Band[{1, 1}] >
      Table[Normal[
        Coefficient[
         Sum[D[1/2 (Subscript[u, n + 1] + Subscript[u,
                   n   1]) + (\[Lambda]   1)*Subscript[u,
                n] + (Subscript[u, n]^2 + \[Beta]*Subscript[v, n]^2)*
                Subscript[u, n] /. {Subscript[u, 1] > Subscript[u,
                1], Subscript[v, 0] > 0,
               Subscript[v, n] > 1*Subscript[v, n],
               Subscript[u, M + 1] > Subscript[u, M]*E^ p,
               Subscript[v, M + 1] > (M + 1)/M*Subscript[v, M]*E^ q},
              Subscript[u, k]]*Subscript[\[Delta]u, k] +
            D[1/2 (Subscript[u, n + 1] + Subscript[u,
                   n   1]) + (\[Lambda]   1)*Subscript[u,
                n] + (Subscript[u, n]^2 + \[Beta]*Subscript[v, n]^2)*
                Subscript[u, n] /. {Subscript[u, 1] > Subscript[u,
                1], Subscript[v, 0] > 0,
               Subscript[v, n] > 1*Subscript[v, n],
               Subscript[u, M + 1] > Subscript[u, M]*E^ p,
               Subscript[v, M + 1] > (M + 1)/M*Subscript[v, M]*E^ q},
              Subscript[v, k]]*Subscript[\[Delta]v, k], {k, 0,
            M + 2}] /. {Subscript[u, 0] > u + Part[deltau, n + 2],
           Subscript[v, 1] > v + Part[deltav, n + 2],
```

```
        Subscript[u, n] -> A*E^( p*Abs[n]) + Part[deltau , n + 2],
        Subscript[u, n   1] ->
         A*E^( p*Abs[n   1]) + Part[deltau , n + 1],
        Subscript[u, n + 1] ->
         A*E^( p*Abs[n + 1]) + Part[deltau , n + 3],
        Subscript[v, n] -> Be*n*E^( q*Abs[n]) + Part[deltav , n + 1],
         Subscript[v, 0] -> 0}, Subscript[\[Delta]u, n],
     1], {Subscript[\[Delta]u, n]}], {n, 0, M}],
Band[{1, 2}] ->
 Table[Normal[
   Coefficient[
    Sum[D[1/2 (Subscript[u, n + 1] + Subscript[u,
              n   1]) + (\[Lambda]   1)*Subscript[u,
            n] + (Subscript[u, n]^2 + \[Beta]*Subscript[v, n]^2)*
            Subscript[u, n] /. {Subscript[u,  1] -> Subscript[u,
            1], Subscript[v, 0] -> 0,
           Subscript[v,  n] -> 1*Subscript[v, n],
           Subscript[u, M + 1] -> Subscript[u, M]*E^ p,
           Subscript[v, M + 1] -> (M + 1)/M*Subscript[v, M]*E^ q},
          Subscript[u, k]]*Subscript[\[Delta]u, k] +
       D[1/2 (Subscript[u, n + 1] + Subscript[u,
              n   1]) + (\[Lambda]   1)*Subscript[u,
            n] + (Subscript[u, n]^2 + \[Beta]*Subscript[v, n]^2)*
            Subscript[u, n] /. {Subscript[u,  1] -> Subscript[u,
            1], Subscript[v, 0] -> 0,
```

```
            Subscript[v,  n] > 1*Subscript[v, n],
            Subscript[u, M + 1] > Subscript[u, M]*E^ p,
            Subscript[v, M + 1] > (M + 1)/M*Subscript[v, M]*E^ q},
           Subscript[v, k]]*Subscript[\[Delta]v, k], {k, 0,
        M + 3}] /. {Subscript[u, 0] > u + Part[deltau , n + 2],
       Subscript[v, 1] > v + Part[deltav , n + 2],
       Subscript[u, n] > A*E^( p*Abs[n]) + Part[deltau , n + 2],
       Subscript[u, n   1] >
        A*E^( p*Abs[n   1]) + Part[deltau , n + 1],
       Subscript[u, n + 1] >
        A*E^( p*Abs[n + 1]) + Part[deltau , n + 3],
       Subscript[v, n] > Be*n*E^( q*Abs[n]) + Part[deltav , n + 1],
        Subscript[v, 0] > 0}, Subscript[\[Delta]u, n + 1],
    1], {Subscript[\[Delta]u, n + 1]}], {n, 0, M   1}],
Band[{2, 1}] >
 Table[Normal[
   Coefficient[
    Sum[D[1/2 (Subscript[u, n + 1] + Subscript[u,
              n   1]) + (\[Lambda]   1)*Subscript[u,
            n] + (Subscript[u, n]^2 + \[Beta]*Subscript[v, n]^2)*
            Subscript[u, n] /. {Subscript[u,  1] > Subscript[u,
            1], Subscript[v, 0] > 0,
           Subscript[v,  n] > 1*Subscript[v, n],
           Subscript[u, M + 1] > Subscript[u, M]*E^ p,
           Subscript[v, M + 1] > (M + 1)/M*Subscript[v, M]*E^ q},
```

```
            Subscript[u, k]]*Subscript[\[Delta]u, k] +
          D[1/2 (Subscript[u, n + 1] + Subscript[u,
                n   1]) + (\[Lambda]   1)*Subscript[u,
              n] + (Subscript[u, n]^2 + \[Beta]*Subscript[v, n]^2)*
              Subscript[u, n] /. {Subscript[u,  1] > Subscript[u,
              1], Subscript[v, 0] > 0,
             Subscript[v,  n] >  1*Subscript[v, n],
             Subscript[u, M + 1] > Subscript[u, M]*E^ p,
             Subscript[v, M + 1] > (M + 1)/M*Subscript[v, M]*E^ q},
            Subscript[v, k]]*Subscript[\[Delta]v, k], {k, 0,
          M}] /. {Subscript[u, 0] > u + Part[deltau , n + 1],
          Subscript[v, 1] > v + Part[deltav , n + 1],
          Subscript[u, n] > A*E^( p*Abs[n]) + Part[deltau , n + 2],
          Subscript[u, n   1] >
           A*E^( p*Abs[n   1]) + Part[deltau , n + 1],
          Subscript[u, n + 1] >
           A*E^( p*Abs[n + 1]) + Part[deltau , n + 3],
          Subscript[v, n] > Be*n*E^( q*Abs[n]) + Part[deltav , n + 1],
           Subscript[v, 0] > 0}, Subscript[\[Delta]u, n   1],
        1], {Subscript[\[Delta]u, n   1]}], {n, 1, M}]}, {M + 1,
    M + 1}];
DU = Join[ConstantArray[0, {1, M}],
   ArrayFlatten[{{SparseArray[{Band[{1, 1}] >
         Table[Normal[
           Coefficient[
```

```
Sum[D[1/
        2 (Subscript[u, n + 1] + Subscript[u,
        n    1]) + (\[Lambda]    1)*Subscript[u,
        n] + (Subscript[u,
        n]^2 + \[Beta]*Subscript[v, n]^2)*Subscript[u,
        n] /. {Subscript[u,  1] > Subscript[u, 1],
       Subscript[v, 0] > 0,
       Subscript[v,  n] >  1*Subscript[v, n],
       Subscript[u, M + 1] > Subscript[u, M]*E^ p,
       Subscript[v,
       M + 1] > (M + 1)/M*Subscript[v, M]*E^ q},
     Subscript[u, k]]*Subscript[\[Delta]u, k] +
   D[1/2 (Subscript[u, n + 1] + Subscript[u,
        n    1]) + (\[Lambda]    1)*Subscript[u,
        n] + (Subscript[u,
        n]^2 + \[Beta]*Subscript[v, n]^2)*Subscript[u,
        n] /. {Subscript[u,  1] > Subscript[u, 1],
       Subscript[v, 0] > 0,
       Subscript[v,  n] >  1*Subscript[v, n],
       Subscript[u, M + 1] > Subscript[u, M]*E^ p,
       Subscript[v,
       M + 1] > (M + 1)/M*Subscript[v, M]*E^ q},
     Subscript[v, k]]*Subscript[\[Delta]v, k], {k, 1,
   M + 2}] /. {Subscript[u, 0] > u + Part[deltau, n + 1],
   Subscript[v, 1] > v + Part[deltav, n + 1],
```

```
  Subscript[u, n] >
   A*E^( p*Abs[n]) + Part[deltau , n + 2],
  Subscript[u, n   1] >
   A*E^( p*Abs[n   1]) + Part[deltau , n + 1],
  Subscript[u, n + 1] >
   A*E^( p*Abs[n + 1]) + Part[deltau , n + 3],
  Subscript[v, n] >
   Be*n*E^( q*Abs[n]) + Part[deltav , n + 1],
  Subscript[v, 0] > 0}, Subscript[\[Delta]v, n],
1], {Subscript[\[Delta]v, n]}], {n, 1, M}]}, {M, M}]}}]]
```

LIST OF REFERENCES

[1] B. A. Malomed and M.I. Weinstein. *Soliton dynamics in the discrete nonlinear Schroedinger equation*, Phys. Lett. A **220**, Issues 1-3, 91-96, (1996).

[2] D. Kincaid, and Ward Cheney, *Numerical Analysis: Mathematics of Scientific Computing*, American Mathematical Society. E 3, (2012).

[3] M. Greiner, O. Mandel, T. Esslinger, T. W. Hansch, I. Bloch, *Quantum Phase Transition from a Superfluid to a Mott Insulator in a Gas of Ultracold Atoms*, Nature **415**, 39-44, (2002).

[4] L. Pitaevskii and S. Stringari, *Bose-Einstein Condensation*, Clarendon Press, Oxford, (2003).

[5] D.J. Kaup, *Variational Solutions for the Discrete Nonlinear Schrödinger Equations*, Mathematics and Computers in Simulation. **69** 322-33, (2005).

[6] G. Herring, P. G. Kevrekidis, B. A. Malomed, R. Carretero-Gonzalez, and D. J. Frantzeskakis, *Symmetry breaking in linearly coupled dynamical lattices*, Phys. Rev. E **76**, 066606, (2007).

[7] P.G. Kevrekidis, *Discrete Nonlinear Schrödinger Equation: Mathematical Analysis, Numerical Computations and Physical Perspectives*, (Springer, Berlin, 2009).

[8] D. E. Pelinovski, *Localization in Periodic Potentials: From Schrödinger Operators to the Gross-Pitaevskii Equations*, Cambridge University Press, Cambridge, (2011).

[9] I. Aslan, *Some exact and explicit solutions to a two-component, discrete, nonlinear Schrödinger model*, Canadian Journal of Physics **89** Issue 8, 857-862, (2011).

[10] C. Chong, D. E. Pelinovsky and G. Schnieder, *Approximation of small-amplitude weakly coupled oscillators with discrete nonlinear Schrödinger*, Physica D **241**, 115, (2012).

[11] B.A. Malomed, D.J. Kaup and R.A. Van Gorder, *Unstaggered-staggered solitons in two-component discrete nonlinear Schrödinger lattices*, Phys. Rev. E **85**, 02664, (2012).

[12] R.A. Van Gorder, B.A. Malomed and D.J. Kaup, *Twisted unstaggered-staggered solitons in two-component discrete nonlinear Schrödinger lattices*, Phys. Rev, (*Unpublished*).